19e Journées de l'Hydrodynamique
26 – 28 novembre 2024, Nantes

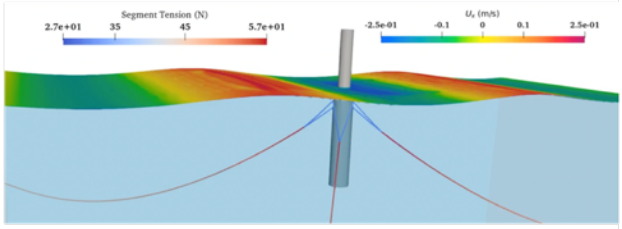

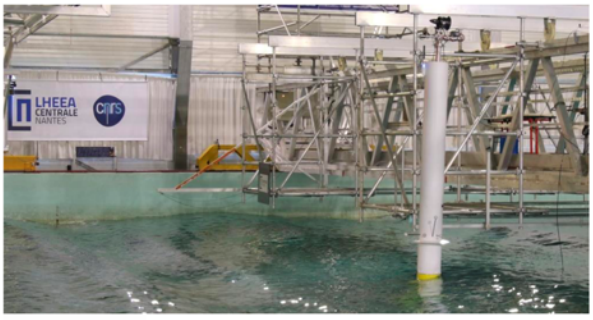

SEAKEEPING SIMULATIONS USING A LEVEL SET APPROACH

Paulin FERRO, Paul LANDEL, Carla LANDRODIE, Marc PESCHEUX
SARL G-MET Technologies
62 rue d'Hyères, 83140 Six-Fours-Les-Plages

ABSTRACT

This study aims at testing the efficiency of a Level-Set solver coded within the OpenFOAM framework (Weller et al. [1998]) to perform ship seakeeping simulations. This solver, named *LSFoam* (Paulin Ferro [2024]), is based on an improved Level-Set method (Sussman et al. [1998]), has a consistent pressure-velocity coupling (Cubero and Fueyo [2007]) and benefits from the Ghost Fluid Method (Fedkiw et al. [1999]). The solver's performances (accuracy and speed) are tested for two test cases: the oscillation of a floating cylinder based on ITO [1971] experiment and the seakeeping experiments of the KCS hull from case 2.10 of the Workshop [2015] (Visonneau et al. [2020]). Simulations are also performed with the standard Volume of Fluid (VoF, Hirt and Nichols [1981]) solver of OpenFOAM: *interFoam*.

***K*eywords** Level Set · Free surface flow · Ghost Fluid Method · OpenFOAM · KCS · Seakeeping · URANS

I – Introduction

Simulations of ship added resistance in waves have become popular due to the need to reduce fossil fuel emissions. During the design stage, simulations can ease the hull shape optimization so that the added resistance effect can be reduced and seakeeping can be improved. Although CFD approaches lead to higher computational costs, compared to potential flow methods, they have gained in popularity due to the increase in computing resources. Open-source codes such as OpenFOAM offer an efficient CFD licence-free framework. The ability of RANS-based CFD methods to produce accurate results for marine applications has been demonstrated at the Workshop [2015] (Visonneau et al. [2020]). The experimental data of the KCS seakeeping, in 5 different sea states, enables researchers to compare their numerical methods and thus, to assist in the development of efficient numerical strategies. Seonguk Seoa [2017] have investigated the results of the OpenFOAM solver *interDyMFoam* coupled with the library *waves2Foam* Jacobsen. They identified some discrepancies for the short wave cases and good agreement with experimental data for the longer ones. Filip et al. [2017] have also calculated the same test cases using OpenFOAM and the *waves2Foam* toolbox Jacobsen et al. [2012]. Correct results are obtained with mean resistance coefficient relative errors below 10%. Lee et al. [2019] have shown that the commercial CFD tool StarCCM+ can also perform the same case with relative errors lower than 10% for the added resistance and below 5% regarding the average trim and sinkage motion responses. Still, for the KCS seakeeping simulations, Vuko and Hrvoje [2015] have performed sensitivity studies using a SWENSE solver Ferrant [2002] that benefits from the Ghost Fluid Method (GFM) Fedkiw et al. [1999] and a level set transport equation derived from phase field equation Sun and Beckermann [2007]. Good agreement was calculated for the case 2.10 and the discrepancy for the oblique wave cases is believed to be caused by experimental issues. Kim and Jun [2021] has presented two VoF-OpenFOAM based solvers texted "*foamStar*" and "*foamStarSWENSE*". Seakeeping simulations have been performed on the Wigley III hull for 3 Froude numbers and 6 wavelengths. The 2.10 KCS wave cases have also been modelled. Using the Euler scheme, "*foamStarSWENSE*" proved to produce more accurate results and better ship motions even though both solvers provide good agreement with experimental data. Some instabilities related to the use of high order Diagonal Implicit Runge-Kutta (DIRK) temporal schemes have been reported. The performances of the classical Level-Set method Sussman et al. [1998] in a CFD finite volume approach to perform such complex simulations have not yet been clearly assessed. Regarding the classical Volume of Fluid method Hirt and Nichols [1981], the level set method is known to have mass conservation issues Sussman et al. [1994]. The proposed method in the *LSFoam* solver Paulin Ferro [2024] has shown excellent performance for complex meshes. The use of the GFM, also implemented in *LSFoam*, has proven to improve wave propagation simulations Ferro et al. [2022] by avoiding light phase accelerations. This study aims to test the efficiency and accuracy of the OpenFOAM based solver *LSFoam* for two test cases. *LSFoam* is first tested for modelling the falling and the oscillation of a floating cylinder. The results are compared with the experimental data of ITO [1971] for three mesh resolutions. The second test case is the modelling of the KCS seakeeping experiment from Workshop [2015], Visonneau et al. [2020]. Regular wave fields are generated with a relaxation zone and ship resistance, sinkage and trim signal harmonic amplitudes are calculated with Fast Fourier Transformations. In this work, the solver numerical procedure is first briefly explained (the reader is referred to Paulin Ferro [2024] for the complete procedure). Then, the floating cylinder test case is presented and finally the KCS seakeeping simulation results are discussed.

II – Mathematical and numerical procedure

II – 1 The Level-Set equation

The interface position is calculated using a Level-Set approach. The Level-Set function $\psi(\boldsymbol{x})$ is defined by the shortest distance d from a point $\boldsymbol{x}$ to the interface. It is signed depending on the point domain (1), so that numerical stability near the interface is improved by avoiding $\boldsymbol{\nabla}\psi$ discontinuities.

$$\psi(\boldsymbol{x}) = \begin{cases} 0 & \boldsymbol{x} \in \Gamma \\ d(\boldsymbol{x}) & \boldsymbol{x} \in \Omega^+ \\ -d(\boldsymbol{x}) & \boldsymbol{x} \in \Omega^- \end{cases} \tag{1}$$

Where the computational domain is divided into two parts: Ω^+ is representing the heavy phase domain, Ω^- the light one and they are separated by the interface Γ. The interface normal $\boldsymbol{n}$ and curvature κ are respectively computed knowing ψ:

$$\boldsymbol{n} = \frac{\boldsymbol{\nabla}\psi}{|\boldsymbol{\nabla}\psi|} \tag{2}$$

$$\kappa = \boldsymbol{\nabla} \cdot \boldsymbol{n} \tag{3}$$

The transport of the Level-Set function in a flow field (assumed incompressible in this work) will breach the distance property and will cause mass variations. A reinitialization procedure is often adopted after the transport by solving the following (eikonal) equation (Sussman et al. [1994]) to recover the distance property:

$$\frac{\partial \psi}{\partial \tau} = S\left(\psi_0\right)\left(1 - |\boldsymbol{\nabla}\psi|\right) \tag{4}$$

Where S is the sign function, ψ_0 the initial value of the level set function before the reinitialization process, and τ has the dimension of a length. The function S is smoothed to improve the numerical resolution near the interface using the expression of Osher and Fedkiw [2003]: $S\left(\psi_0\right) = \frac{\psi_0}{\sqrt{\psi_0^2 + |\boldsymbol{\nabla}\psi_0|\epsilon(\boldsymbol{x})^2}}$ where $\epsilon(\boldsymbol{x})$ is the filtering length defined below. Sussman et al. [1998] defined $\boldsymbol{w} = S\left(\psi_0\right)\boldsymbol{n}$, which leads to the following form of the reinitialization equation:

$$\frac{\partial \psi}{\partial \tau} + \boldsymbol{\nabla} \cdot (\boldsymbol{w}\psi) - \psi \boldsymbol{\nabla} \cdot \boldsymbol{w} = S\left(\psi_0\right) \tag{5}$$

Equation 5 is more suitable for implicit finite volume discretization Vukcevic and Jasak [2014], facilitating the use of unstructured meshes and improving the numerical stability. However, in practice, interface displacements can still occur during the reinitialization procedure, leading to unacceptable mass variations. Having a reinitialization frequency and/or iteration number that is too high can result in significant interface displacements. Thus, determining the optimal iteration number and frequency for a given test case is the major drawback of this method. To address these issues, equation 5 is solved using the method defined in Paulin Ferro [2024]:

- A Local Time Stepping approach (LTS) is employed where the spatial time step τ is adjusted locally based on a given maximal reinitialization Courant number, γ_{max}:

$$\frac{1}{\tau\left(\boldsymbol{x}\right)} = max\left(\frac{1}{\Delta z\left(\boldsymbol{x}\right)}, \frac{\sum\limits_{f} \boldsymbol{w}_f \cdot \boldsymbol{S}_f}{\gamma_{max} V\left(\boldsymbol{x}\right)}\right) \tag{6}$$

  Where $\boldsymbol{w}_f$ is obtained by linear interpolation of $\boldsymbol{w}$ from cell center to face center. The spatial time step $\tau(\boldsymbol{x})$ is maximised for each cell based on γ_{max} but can't exceed the local cell size $\Delta z\left(\boldsymbol{x}\right)$.

- Anchoring cells are defined to avoid any interface displacements during the resolution of the reinitialization. The set of cells (called anchoring cells) that cross the zero Level-Set contour are detected (they share a face that satisfies $\psi_O \psi_N < 0$). The corresponding Level-Set values are stored before the reinitialization procedure. Then, after each iteration of the reinitialization process, Level-Set values of the anchoring cells are restored so that the zero Level-Set contour remains undisturbed.
- The filtering length $\epsilon(\boldsymbol{x})$ is non-uniform and depends on the local cell size. $\epsilon(\boldsymbol{x}) = kl_e$ with k a user defined constant (usually $k = 2$) and $l_e(x)$ the length of the cell edge that have the highest scalar product with the interface normal vector.

The Level-Set function is used to calculate the volume fraction α by applying the standard hyperbolic filtering function:

$$\alpha = \frac{1}{2}\left(tanh\left(\frac{\pi\psi}{\epsilon(\boldsymbol{x})}\right) + 1\right) \tag{7}$$

The phase fraction α is then used to calculate the mixture viscosity μ and the densities as:

$$\mu = \alpha\mu^+ + (1 - \alpha)\,\mu^- \tag{8}$$

$$\begin{cases} \rho = \rho^+ & if\ \psi > 0 \\ \rho = \rho^- & if\ \psi < 0 \end{cases} \tag{9}$$

Where $\mu^+$and μ^- are the dynamic viscosity of heavy and light phases and ρ^+ and ρ^- their density.

II – 2 Consistent pressure-velocity coupling

The non-conservative momentum equation form is adopted:

$$\frac{\partial \boldsymbol{u}}{\partial t} + \boldsymbol{\nabla} \cdot (\boldsymbol{u} \otimes \boldsymbol{u}) = \frac{1}{\rho} \left(\boldsymbol{\nabla} p_d + \boldsymbol{\nabla} \cdot \left[\mu_{eff} (\nabla \boldsymbol{u} + (\nabla \boldsymbol{u})^T) - \mu_{eff} \frac{2}{3} \mathrm{tr}(\nabla \boldsymbol{u})^T \right] \right), \; in \; \Omega^+ \; or \; \Omega^- \tag{10}$$

Where $\boldsymbol{u}$ is the velocity field, μ_{eff} the effective viscosity (sum of the molecular viscosity μ and turbulence viscosity μ_{turb}) and p_d the piezometric pressure $p_d = p - \rho \boldsymbol{g} \cdot \boldsymbol{x}$, Rusche [2002]. Having a continuous velocity and dynamic viscosity fields, equation 10 is completed by the following set of jump conditions at the interface Γ:

$$\left[\frac{\boldsymbol{\nabla} p_d}{\rho} \right]_\Gamma = 0 \tag{11}$$

$$[p_d]_\Gamma = \sigma \kappa + [\rho]_\Gamma \, \boldsymbol{g} \cdot \boldsymbol{x}_\Gamma = \mathcal{H} \tag{12}$$

Where $\boldsymbol{x}_\Gamma$ is the interface coordinate vector and σ the surface tension coefficient. The bracket notation $[.]_\Gamma$ indicates a jump value between both sides of the interface. The momentum equation 10 is discretized without the pressure gradient term. The remaining terms are treated implicitly excepting $\frac{1}{\rho} \boldsymbol{\nabla} \cdot \left[\mu_{eff} (\nabla \boldsymbol{u})^T - \mu_{eff} \frac{2}{3} \mathrm{tr}(\nabla \boldsymbol{u})^T \right]$. The semi-discretized momentum equation takes the following form for cell P surrounded by neighbour N:

$$a_P \boldsymbol{u}_P = -\frac{\boldsymbol{\nabla} p_d}{\rho} - \sum_f a_N \boldsymbol{u}_N + \boldsymbol{s}(\boldsymbol{u}) = -\frac{\boldsymbol{\nabla} p_d}{\rho} + \boldsymbol{H}(\boldsymbol{u}_P) \tag{13}$$

Where a_P and a_N are respectively the diagonal and off-diagonal coefficients. To avoid checkerboard oscillations on collocated grids, the so-called Rhie and Chow [1983] interpolation is used to obtain the face velocity by mimicking Equation 13. In this work, to avoid relaxation and time step dependencies the interpolation of each term is performed in a consistent manner following Cubero and Fueyo [2007]. The coefficient a_P is decomposed into its temporal a_t and spatial a_s parts. The old time contribution is taken out from $\boldsymbol{H}(\boldsymbol{u})$ (first order *Euler* scheme here as an example) and relaxation is applied to Equation 13, resulting in:

$$\boldsymbol{u}_P = \frac{1}{1+d} \left(-\frac{\alpha_u}{a_s} \frac{\boldsymbol{\nabla} p_d}{\rho} + \frac{\alpha_u}{a_s} \boldsymbol{H}(\boldsymbol{u}_P) + \alpha_u d \boldsymbol{u}_P^0 \right) + (1 - \alpha_u) \boldsymbol{u}_P^{k-1} \tag{14}$$

Where $d = \frac{a_t}{a_s}$, α_u is the relaxation factor, $\boldsymbol{u}_P^{k-1}$ the velocity field of the previous non linear iteration (PIMPLE loop), and $\boldsymbol{u}_P^0$ the previous time step velocity field. The face velocity equation is then obtained by mimicking Equation 14 at faces (written in term of flux ϕ [m^3/s]).

$$\phi_f = \frac{1}{1 + [d]_f} \left(-\left[\frac{\alpha_u}{a_s} \right]_f \left(\frac{\boldsymbol{\nabla} p_d}{\rho} \right)_f + \left[\frac{\alpha_u \boldsymbol{H}(\boldsymbol{u}_p)}{a_s} \right]_f \cdot \boldsymbol{S}_f + \alpha_u [d]_f \phi_f^0 \right) + (1 - \alpha_u) \phi_f^{k-1} \tag{15}$$

Where $[.]_f$ is the operator that linearly interpolates from the cell center to the face center. The continuity equation is then applied to Equation 15 to obtain the pressure Poisson equation in its finite volume discretized form:

$$\sum_f \frac{\left[\frac{\alpha_u}{a_s} \right]_f}{1 + [d]_f} \left(\frac{\boldsymbol{\nabla} p_d}{\rho} \right)_f \cdot \boldsymbol{S}_f = \sum_f \frac{1}{1 + [d]_f} \left(\left[\frac{\alpha_u \boldsymbol{H}(\boldsymbol{u}_p)}{a_s} \right]_f \cdot \boldsymbol{S}_f + \alpha_u [d]_f \phi_f^0 \right) + \sum_f (1 - \alpha_u) \phi_f^{k-1} \tag{16}$$

The mesh non-orthogonality is handled using the over-relaxed approach, Jasak [1996]. The surface vector $\boldsymbol{S}_f$ is decomposed in two parts: the orthogonal $\boldsymbol{\delta}$ discretized implicitly, and the non-orthogonal $\boldsymbol{k}$ treated explicitly. After solving the pressure Poisson equation, the velocity field and conservative face flux ϕ are respectively updated using Equations 14 and 15 with the updated pressure field. The jump conditions 11 and 12 are employed to derive interface corrected interpolation schemes in the manner of Vukcevic [2016a], where the procedure is given in details.

II – 3 Solver chart of *LSFoam*

The Level-Set, momentum, and pressure Poisson equations are solved in a segregated manner with the PIMPLE algorithm available in OpenFOAM. The PIMPLE algorithm is a combination of SIMPLE (Patankar and Spalding [1972]) and PISO (Patankar and Spalding [1972], Issa [1986]) algorithms. The steps are described below 1.

```
while t < t_end do:
    do PIMPLE loop:
        Call dynamic mesh motion
        Update grid and flux
        Solve the Level-Set transport equation

        if last PIMPLE loop:
            Solve the eikonal reinitialization Level-Set equation 5

        Apply relaxation zone on ψ and u
        Update ρ and μ
        Update GFM jump conditions
        Build velocity equation 13

        do PISO:
            Solve Pressure Poisson equation 16
            Update flux and velocity

        Solve turbulence equations
```

Listing 1: Segregated LSFoam flow algorithm

III – The falling of a floating cylinder, ITO [1971]

The falling of a solid floating cylinder in water has been simulated following the experiment of ITO [1971]. This test case has also been performed by Filip et al. [2017], Wang and Al. [2019], Chen et al. [2019] and Joshi et al. [2018]. A cylinder with a diameter of $d = 0.1524$ m is placed at $y_0 = d/6$ above the free surface without initial velocity. The cylinder has a density of $500\ kg/m^3$. The 2D numerical domain is illustrated in Figure 1. Its length is $50d$ and the water depth equals $7.9d$. The waves generated by the falling cylinder are damped close to the side patches with relaxation zones so that any potential reflections are avoided. The bottom patch is a wall. The top patch is an atmospheric boundary condition. A mesh sensitivity study has been performed with three meshes composed of 37k, 54k and 138k cells. The three grids have been generated by *snappyHexMesh* and are illustrated in Figure 2. The simulations are performed with an adaptable time step based on a maximum CFL condition of 0.3. The temporal terms are resolved using the *backward* scheme. Six outerCorrectors (SIMPLE) and six correctors (PISO) are used. Convective terms are discretized with the *linearUpwind* scheme, and the corresponding gradients are calculated using the *Gauss linear* scheme, except for the pressure one, which is calculated using the *leastSquares* method (corrected through GFM). The history of the cylinder's center of mass position is compared with the experimental data from ITO [1971] in Figure 3. Excellent agreement is found for the finest grid, whereas having a coarser mesh tends to dampen the oscillations. Results for the finest grid are also compared with those from *interFoam*. The numerical settings are the same except for the temporal scheme, calculated with the *CrankNicolson 0.5*, as the *backward* is not available with *interFoam*. The results from both solvers are really close to the experimental data, but the main difference between the two solvers for this test case is the calculation time, summarized in table 1. The *LSFoam* simulations for the medium and fine grids lasted 1h34 and 8 hours on 4 cores, while for *interFoam*, with the same number of cores, they lasted 1h50 and 11 hours. Having a finer mesh tends to increase the calculation time difference as it also tends to create more spurious air velocities with *interFoam*.

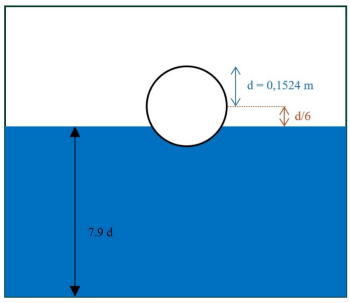

Figure 1: Illustration of the ITO [1971] test case

LSFoam Coarse	*LSFoam* Medium	*LSFoam* Fine	*interFoam* Coarse	*interFoam* Medium	*interFoam* Fine
0h36	1h34	8h	0h45	1h50	11h18

Table 1: Calculation times for *LSFoam* and *interFoam* on 4 cores

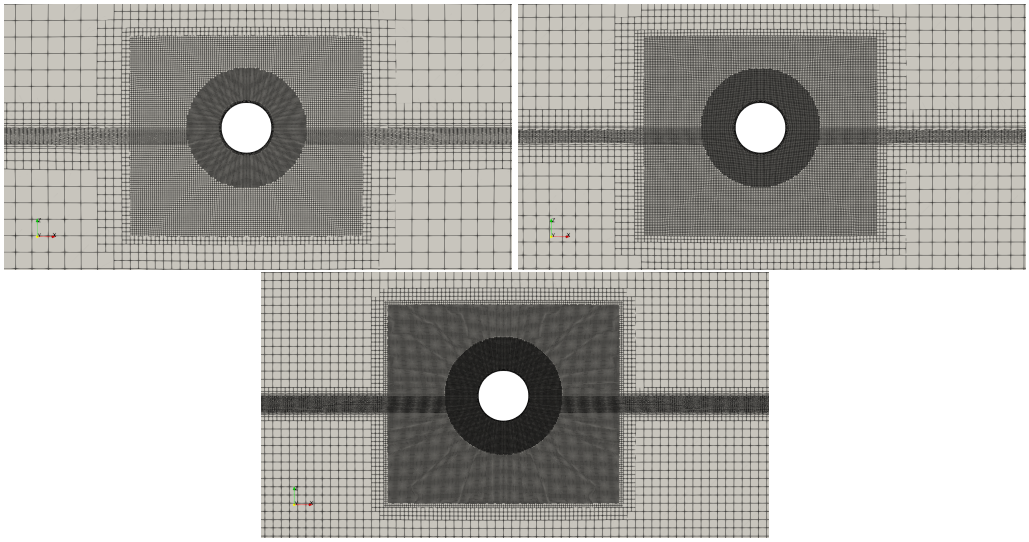

Figure 2: coarse, medium and fine grids

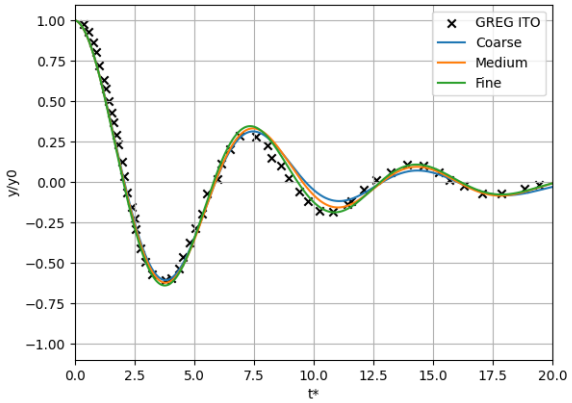

Figure 3: *LSFoam* results for the three meshes

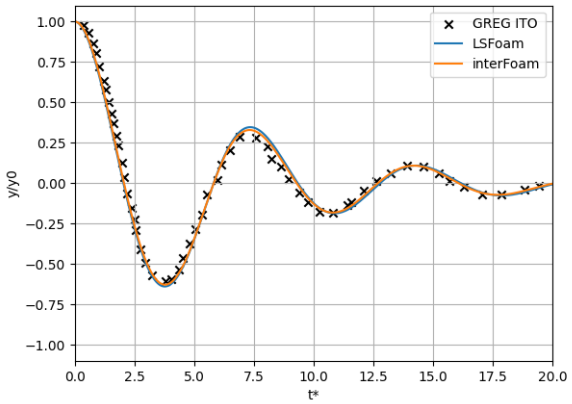

Figure 4: Results comparison between *interFoam* and *LSFoam* for the finest grid

IV – Workshop [2015] (Visonneau et al. [2020]) case 2.10, KCS seakeeping simulations

Figure 5: KCS geometry

This test case consists in modelling the KRISO Container Ship (KCS) behaviour in different regular head wave configurations. The KCS is designed by the Korean Research Institute of Ship and Ocean Engineering (KRISO) and is illustrated in Figure 5. Both the experiments and the simulations are performed with a scaled ship (LPP = 6,07 m) including a rudder. Its main particular is summarized in table 2. The five configurations from the case 2.10 of the 2015 Workshop [2015] (Visonneau et al. [2020]) have been simulated, Table 4. The 2.07 m/s ship's velocity is the same for all the test cases and corresponds to a Froude number of 0.261. The higher the configuration number, the longer the wave length. Case C_0 corresponds to calm water and case C_3 to the resonance domain. The numerical towing tank is illustrated in Figure 6 and is composed of two relaxation zones for wave management: one for generation at the inlet and one for damping at the outlet. Simulations are carried out in the fixed ship reference frame using stream function wave theory, Fenton [1990]. A symmetry condition is applied on the $y = 0$ plane. Turbulence effects are simulated with the $k - \omega$ SST model, Menter et al. [2003]. The air/water flow is imposed at the entrance of the computational domain within the inlet relaxation zone. A pressure reference is imposed at the top via an atmospheric boundary condition. For the bottom and lateral patches, a slip condition is used, while at the outlet, a zero-gradient condition is applied. Wall functions are used for the hull patch. The grids are generated with *snappyHexMesh*, and the near-hull region meshes are illustrated in Figure 7. In this region, cells are refined in each direction within a rectangular box. Close to the free surface, the cells are refined between -1 m and +1 m in all directions.

Calm Water case C_0:

A mesh sensitivity study was conducted on the calm water case (C_0). Three meshes were generated. The coarse mesh contains 0.86 M cells, the medium mesh 1.9 M cells, and the fine one 3.7 M cells. Simulations were performed using both *LSFoam* and *interFoam* with a fixed time step of 25 ms over a period of 50 s. The results of this sensitivity study are presented in table 3. The drag coefficient C_T is calculated from the force history:

$$C_T = \frac{F_x}{0.5\rho U^2 S_w}$$

The trim (in degree) and sinkage (divided by L_{pp}) are also calculated. Both medium and fine mesh results have excellent agreement with the experimental data for both solvers, with relative errors lower than 5%. The calculation durations are longer with *interFoam*. The medium mesh provides a good balance between computational cost and accuracy. Based on this study, the medium mesh will be used for the wave cases. The numbers of cells per wave height, per wave length, and the number of time step per period are listed in table 5.

Head wave cases $C_{1/2/3/4/5}$:

Simulations are performed with a fixed time step of 10 ms, and the temporal terms are discretized using the first-order implicit Euler scheme. Six outerCorrectors (SIMPLE) and five correctors (PISO) are used. Fast Fourier Transformations (FFT) are calculated on the resistance, trim and sinkage signals. The five sea states are illustrated in Figure 8. Mean values and the first peak amplitudes are calculated for both *interFoam* and *LSFoam*, and they are compared with the experimental data reported in Visonneau et al. [2020]. The trim values (in degree) are divided by the wave steepness $Ak = kHs/2$n, and the sinkage values are divided by $A = Hs/2$. Regarding resistance, the mean and first harmonic amplitudes are plotted in Figure 9. The mean values calculated by *LSFoam* (shown in table 6) are close to the experimental data, with relative errors lower than 5%, except for the C_3 test case that correspond to the resonance domain with a relative error of 9%. For the first harmonic, the calculated amplitudes are underestimated for both *interFoam* and *LSFoam*. The same trend is also observed in Vukcevic [2016b] and Filip et al. [2017]. For the dimensionless trim (Figure 10 and table 7), the overall trend is captured with reasonable agreement for both mean and

first harmonic values. The mean values show medium agreement with experimental data, excepting for the cases C_3 (resonating) and C_4, where the errors are significant. For *interFoam*, the last case also exhibits an important relative error (> 50 %). The first harmonic amplitudes are underestimated for both solvers, with mainly larger errors for *interFoam*. Finally, regarding the dimensionless sinkage (Figure 11 and table 8), the trends are in overall good agreement with experimental data for both medium and first harmonic values. *interFoam* performs slightly better for the mean values, with a maximum relative error of -21 % for the fourth case. The first harmonic amplitudes are underestimated for the first three cases, but a good agreement is found for the last two cases with *LSFoam*, showing relative errors of ≈ 3 % and ≈ 0.5 %.

Figure 6: The computational domain

	Full scale	Model
Length between perpendiculars $L_{PP}(m)$	230.0	6.07
Length of waterline $L_{WL}(m)$	232.5	6.13
Draft T (m)	10.8	0.285
Displacement volume $\Delta(m^3)$	52030	0.9571
Wetted surface area with rudder $S(m^2)$	9539	6.6978
Moment of inertia $K_{yy}/L_{pp}, K_{zz}/L_{pp}$,	0.250	0.252

Table 2: KCS main particular

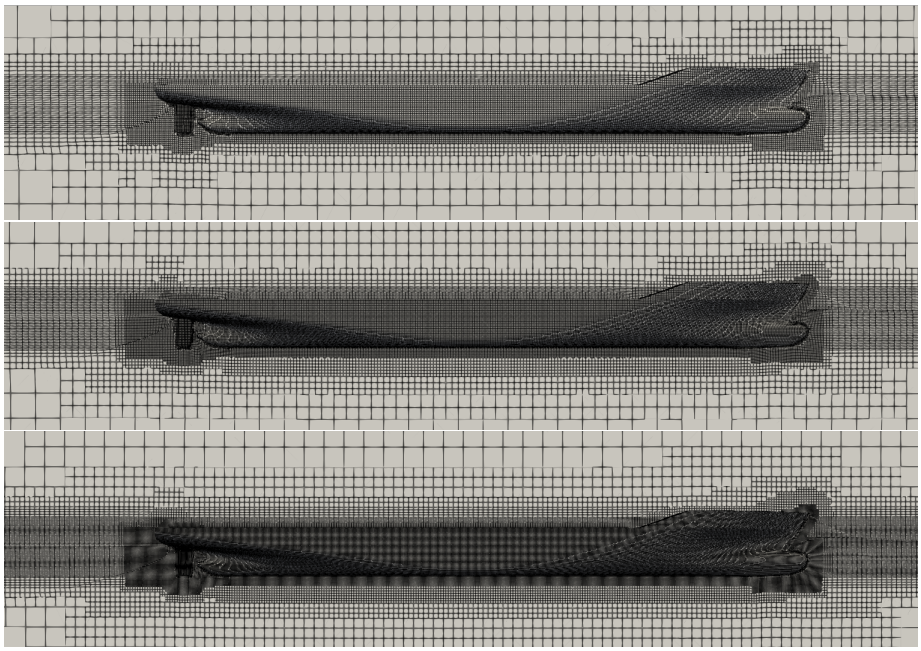

Figure 7: The three grids used for the sensitivity study. From top to bottom: coarse, medium and fine

		C_T	$z/L_{pp}10^-3$	$\theta(^\circ)$	$Err_{C_t}(\%)$	$Err_z(\%)$	$Err_\theta(\%)$	CPU time
$LSFoam$	Coarse	4.017	-2.022	-0.1670	4.7	-2.3	1.4	3h23
	Medium	3.871	-2.014	-0.1707	0.94	-2.7	3.7	7h02
	Fine	3.864	-2.025	-0.1674	0.75	-2.2	1.7	12h18
$interFoam$	Coarse	4.068	-2.063	-0.166	6.1	-0.3	0.7	4h43
	Medium	3.936	-2.030	-0.163	2.6	-1.9	-1.1	8h40
	Fine	3.800	-2.047	-0.165	-0.9	-1.06	0.23	14h19
Experimental data		3.835	-2.074	-0.1646				

Table 3: C_0 sensitivity study results

	C_0	C_1	C_2	C_3	C_4	C_5
speed (m/s)	2.07					
Froude number (Fr)	0.261					
Reynolds Number (R_{ey})	1.074×107					
Wave length (λ/L_{pp})	Na	0.65	0.85	1.15	1.37	1.95
Wave height: Hs (m)	Na	0.062	0.078	0.123	0.149	0.196
Wave steepness Ak	Na	0.049	0.047	0.055	0.056	0.052

Table 4: Case wave conditions

	C_1	C_2	C_3	C_4	C_5
number of cells per wave height	3.8	4.9	7.7	9.3	12.2
number of cells per wave length	9.15	12.0	16.2	19.3	27.5
number of time step per wave period	88	106	131	148	187

Table 5: Incident wave time and space discretization for medium grid

Case	*LSFoam*		*interFoam*	
	Mean, Err_{C_T}	h1, Err_{C_T}	Mean, Err_{C_T}	h1, Err_{C_T}
C_1	0.6	-60.9	9.0	-56.9
C_2	-4.3	-27.6	1.6	-32.2
C_3	-9.1	-4.8	-9.5	-12.7
C_4	-0.9	-28.9	1.1	-40.7
C_5	0.46	-8.7	4.9	-15.0

Table 6: Resistance coefficient mean value and first harmonic amplitude relative errors for both solver

Case	*LSFoam*		*interFoam*	
	Mean, $Err_{\theta/Ak}$	h1, $Err_{\theta/Ak}$	Mean, $Err_{\theta/Ak}$	h1, $Err_{\theta/Ak}$
C_1	4.4	-48.8	11.1	-47.5
C_2	13.6	6.0	3.0	-9.7
C_3	3800	-22.0	4500	-30.6
C_4	68.5	-21.7	137.8	-28.4
C_5	12.3	-6.2	50.4	-13.5

Table 7: Dimensionless trim mean value and first harmonic amplitude relative errors for both solver

Case	*LSFoam*		*interFoam*	
	Mean, $Err_{z/A}$	h1, $Err_{z/A}$	Mean, $Err_{z/A}$	h1, $Err_{z/A}$
C_1	-12.3	-63.0	-9.9	-57.5
C_2	-14.1	-33.8	-8.4	-49.4
C_3	-4.6	-14.6	7.3	-28.5
C_4	-33.1	-2.7	-21.4	-3.3
C_5	-39.7	-0.6	-14.3	-7.4

Table 8: Dimensionless sinkage mean value and first harmonic amplitude relative errors for both solver

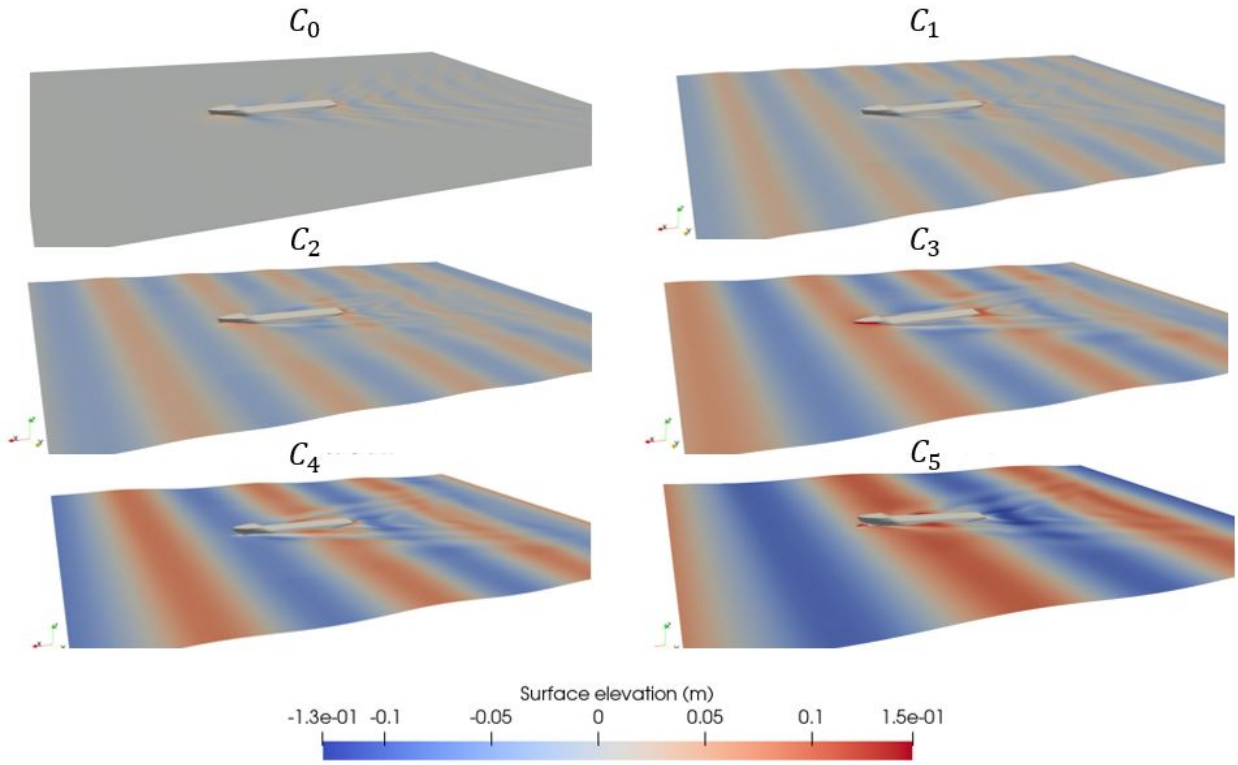

Figure 8: View of the sea states

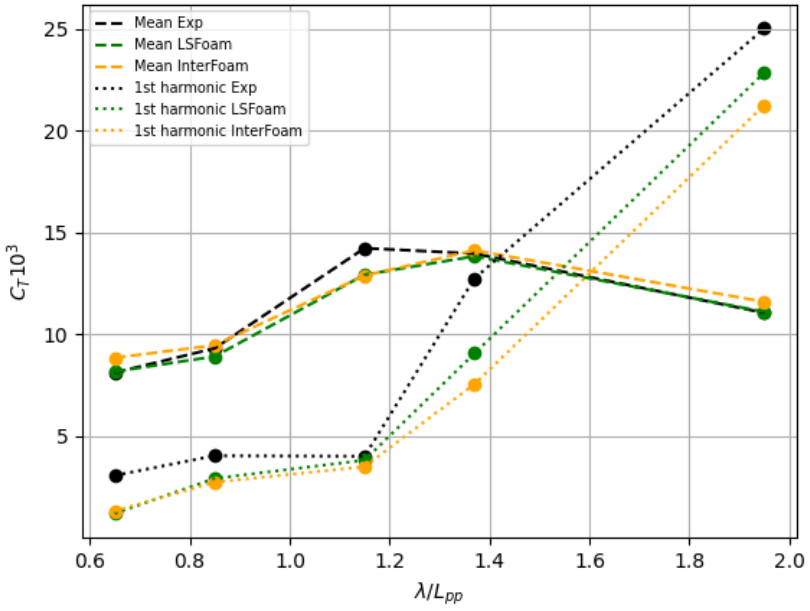

Figure 9: Resistance coefficient values for all wave conditions

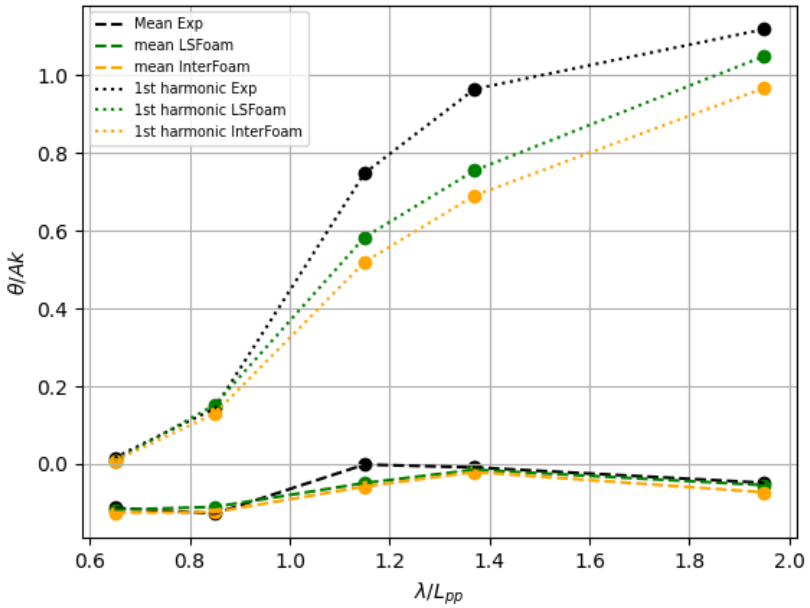

Figure 10: Dimensionless trim values for all wave conditions

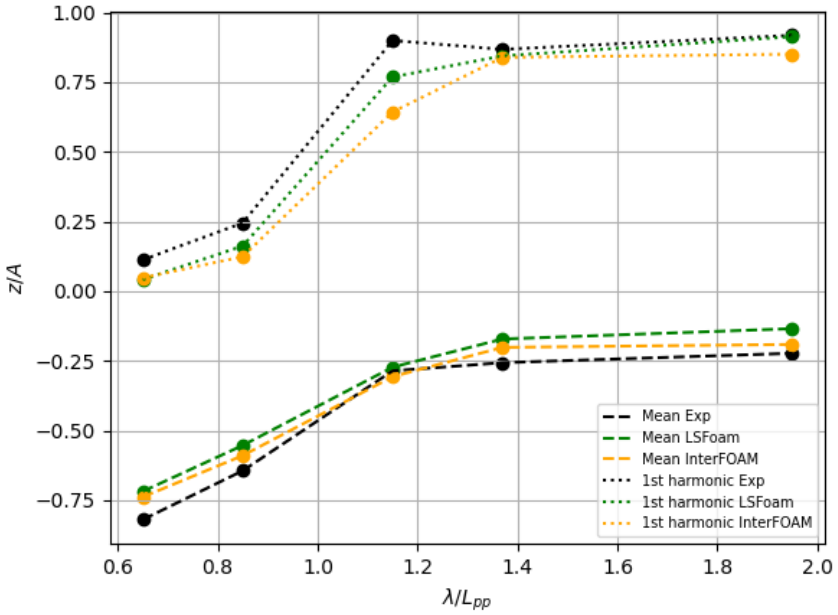

Figure 11: Dimensionless sinkage values for all wave conditions

V – Conclusions

Seakeeping and added resistance simulations are valuable during a hull design stage. However, they remain challenging to model with CFD approaches compared to the classical, but less accurate, potential flow methods. The CFD solver, proposed by Paulin Ferro [2024], employs a coupled Level-Set method / Ghost Fluid Method (GFM), with a time consistent pressure-velocity coupling as described by Cubero and Fueyo [2007] and an enhanced reinitialization procedure. First, the falling of a floating cylinder is simulated following the experiment by ITO [1971]. Both *interFoam* and *LSFoam* showed good agreement with the experimental data. However, *LSFoam* is computationally less expensive. Then, the test case 2.10 from 2015 Tokyo workshop (Workshop [2015], Visonneau et al. [2020]) is reproduced. A mesh sensitivity study is conducted on the calm water resistance case (C_0) to achieve an optimal balance between computational cost and accuracy. Simulations are then performed for both *interFoam* and *LSFoam*. Overall good agreements with experimental data are observed for the resistance mean values. The relative errors are below 10 %. For trim and sinkage motions, average values range from good to poor agreement (especially for the resonating case). The first harmonic amplitudes are calculated using Fast Fourier Transformations (FFT). The resistance coefficient first harmonic amplitudes are underestimated for both solvers, with a maximum relative error of 60% for case C1 (both solver). Regarding the motions, the first harmonic amplitudes range from excellent to poor agreement depending on the case. *LSFoam* and *interFoam* provide results with important errors that are likely due to insufficient mesh and/or time step resolution. It has to be noticed that the KCS inertia moment I_{yy} could play an important role in the motion responses and its influence has not been assessed.

VI – Declaration of competing interests

The authors declare that they have no known competing financial.

References

W. Chen, Z. Deng, W. Pinjie, and Y. Yao. Wave power extraction from a dual oscillating-water- column system composed of heave-only and onshore units. *Energies*, 12, 05 2019. doi: 10.3390/en12091742.

A. Cubero and N. Fueyo. A compact momentum interpolation procedure for unsteady flows and relaxation. *Numerical Heat Transfer, Part B: Fundamentals*, 52(6):507–529, 2007. doi: 10.1080/10407790701563334. URL https://doi.org/10.1080/10407790701563334.

R. P. Fedkiw, T. Aslam, and S. Xu. The ghost fluid method for deflagration and detonation discontinuities. *Journal of Computational Physics*, 154(2), 9 1999. ISSN 0021-9991. doi: 10.1006/jcph.1999.6320. URL https://www.osti.gov/biblio/20000635.

J. D. Fenton. Nonlinear wave theories. *Wiley, Ch. 1, pp. 325, from The Sea. Ideas and Observations on Progress in the Study of the Seas. Part A. Editors: B. Le Méhauté and D. M. Hanes.*, 1990.

G. L. L. T. D. Ferrant, P. A new ranse/potential approach for water wave diffraction. *In: Proceedings of Numerical Towing Tank Symposium,NuTTS, September.*, 2002.

P. Ferro, P. Landel, M. Pescheux, and S. Guillot. Development of a free surface flow solver using the ghost fluid method on openfoam. *Ocean Engineering*, 253:111236, 2022. ISSN 0029-8018. doi: https://doi.org/10.1016/j.oceaneng.2022.111236. URL https://www.sciencedirect.com/science/article/pii/S0029801822006321.

Filip, Xu, and Maki. Urans predictions of resistance and motions of the kcs in head waves. 2017.

C. Hirt and B. Nichols. Volume of fluid (vof) method for the dynamics of free boundaries. *Journal of Computational Physics*, 39(1):201–225, 1981. ISSN 0021-9991. doi: https://doi.org/10.1016/0021-9991(81)90145-5. URL https://www.sciencedirect.com/science/article/pii/0021999181901455.

R. Issa. Solution of the implicitly discretised fluid flow equations by operator-splitting. *Journal of Computational Physics*, 62(1):40–65, 1986. ISSN 0021-9991. doi: https://doi.org/10.1016/0021-9991(86)90099-9. URL https://www.sciencedirect.com/science/article/pii/0021999186900999.

ITO. Study of the transient heave oscillation of a floating cylinder. 1971.

N. F. D. F. J. . Jacobsen. A wave generation toolbox for the open-source cfd library: Openfoam. *Int. J. Numer. Methods Fluids 70*.

N. G. Jacobsen, D. R. Fuhrman, and J. Fredsøe. A wave generation toolbox for the open-source cfd library: Openfoam®. *International Journal for Numerical Methods in Fluids*, 70(9):1073–1088, 2012. doi: https://doi.org/10.1002/fld.2726. URL https://onlinelibrary.wiley.com/doi/abs/10.1002/fld.2726.

H. Jasak. *Error Analysis and Estimation for the Finite Volume Method with Applications to Fluid Flows*. PhD thesis, 1996.

V. Joshi, P. Saradhi, Y. Z. Law, and P. Adaikalaraj. A 3d coupled fluid-flexible multibody solver for offshore vessel-riser system. page V002T08A009, 06 2018. doi: 10.1115/OMAE2018-78281.

Kim and Y. Jun. *Numerical improvement and validation of a naval hydrodynamics CFD solver in view of performing fast and accurate simulation of complex ship-wave interaction.* Theses, École centrale de Nantes, July 2021. URL https://theses.hal.science/tel-03530266.

Y.-G. Lee, C. Kim, J.-H. Park, H. Kim, I. Lee, and B. Jin. Numerical simulations of added resistance in regular head waves on a container ship. *Brodogradnja*, 70:61–86, 06 2019. doi: 10.21278/brod70204.

F. R. Menter, M. Kuntz, R. Langtry, K. Hanjalic, Y. Nagano, and M. J. Tummers. Ten years of industrial experience with the sst turbulence model, 4th:; internal symposium, turbulence, heat and mass transfer. In *TURBULENCE HEAT AND MASS TRANSFER, Turbulence, heat and mass transfer, 4th:; Internal Symposium, Turbulence, heat and mass transfer*, volume 4, pages 625–632, New York, 2003. Begell House,;. ISBN 1567001963. URL https://www.tib.eu/de/suchen/id/BLCP%3ACN053216624.

S. J. Osher and R. Fedkiw. *Level set methods and dynamic implicit surfaces.*, volume 153 of *Applied mathematical sciences*. Springer, 2003. ISBN 0387954821.

S. Patankar and D. Spalding. A calculation procedure for heat, mass and momentum transfer in three-dimensional parabolic flows. *International Journal of Heat and Mass Transfer*, 15(10):1787–1806, 1972. ISSN 0017-9310. doi: https://doi.org/10.1016/0017-9310(72)90054-3. URL https://www.sciencedirect.com/science/article/pii/0017931072900543.

C. L. Paulin Ferro, Paul Landel. Enhanced level-set method for free surface flow applications. 2024.

C. M. Rhie and W. L. Chow. Numerical study of the turbulent flow past an airfoil with trailing edge separation. *AIAA Journal*, 21(11):1525–1532, 1983. doi: 10.2514/3.8284. URL https://doi.org/10.2514/3.8284.

H. Rusche. *Computational Fluid Dynamics of Dispersed Two-Phase Flows at High Phase Fractions*. PhD thesis, Imperial College, London, 2002. URL http://powerlab.fsb.hr/ped/kturbo/OpenFOAM/docs/HenrikRuschePhD2002.pdf.

B. K. Seonguk Seoa, Sunho Parka. Effect of wave periods on added resistance and motions of a ship in head sea simulations. *Ocean Engineering*, 2017.

Y. Sun and C. Beckermann. Sharp interface tracking using the phase-field equation. *Journal of Computational Physics*, 220(2):626–653, 2007. ISSN 0021-9991. doi: https://doi.org/10.1016/j.jcp.2006.05.025. URL https://www.sciencedirect.com/science/article/pii/S0021999106002531.

M. Sussman, P. Smereka, and S. Osher. A level set approach for computing solutions to incompressible two-phase flow. *Journal of Computational Physics*, 114(1):146–159, 1994. ISSN 0021-9991. doi: https://doi.org/10.1006/jcph.1994.1155.

M. Sussman, E. Fatemi, P. Smereka, and S. Osher. An improved level set method for incompressible two-phase flows. *Computers and Fluids*, 27(5):663–680, 1998. ISSN 0045-7930. doi: https://doi.org/10.1016/S0045-7930(97)00053-4. URL https://www.sciencedirect.com/science/article/pii/S0045793097000534.

M. Visonneau, T. Hino, F. Stern, and L. Larson. *An assessment of the Tokyo 2015 Workshop*. 2020. doi: 10.1007/978-3-030-47572-7. URL https://hal.science/hal-03124565.

V. Vukcevic. *Numerical Modelling of Coupled Potential and Viscous Flow for Marine Applications*. PhD thesis, 11 2016a.

V. Vukcevic. Numerical modelling of coupled potential and viscous flow for marine applications. *University of Zagreb, Faculty of Mechanical Engineering and Naval Architecture*, 2016b.

V. Vukcevic and H. Jasak. A conservative level set method for interface capturing in two-phase flows. 2014.

V. Vuko and J. Hrvoje. Seakeeping validation and verification using decomposition model based on embedded free surface method. *Faculty of Mechanical Engineering and Naval Architecture*, 2015.

D. Wang and Al. Extended variable-time-step adams–bashforth–moulton method for strongly coupled fluid–structure interaction simulation. *Ocean Engineering*, 2019.

H. G. Weller, G. Tabor, H. Jasak, and C. Fureby. A tensorial approach to computational continuum mechanics using object-oriented techniques. *Computers in Physics*, 12(6):620–631, 1998. doi: 10.1063/1.168744. URL `https://aip.scitation.org/doi/abs/10.1063/1.168744`.

T. Workshop. Tokyo 2015: A workshop on cfd in ship hydrodynamics. In *Tokyo 2015: A Workshop on CFD in Ship Hydrodynamics*, 2015.